Journal of Materials Science & Technology 176 (2024) 112–118

Contents lists available at ScienceDirect

Journal of Materials Science & Technology

journal homepage: www.elsevier.com/locate/jmst

Research Article

Single-crystallization of electrolytic copper foils

Xingguang Li[a], Mengze Zhao[a], Quanlin Guo[a], Chong Zhao[b], Mingchao Ding[c], Dingxin Zou[d], Zhiqiang Ding[b], Zhiqiang Zhang[b], Menglin He[b], Kehai Liu[b], Muhong Wu[e], Zhihong Zhang[f], Enge Wang[b,e], Ying Fu[b,*], Kaihui Liu[a,b,e,*], Zhibin Zhang[a,*]

[a] State Key Laboratory for Mesoscopic Physics, Frontiers Science Centre for Nano-optoelectronics, School of Physics, Peking University, Beijing 100871, China
[b] Songshan Lake Materials Laboratory, Dongguan 523808, China
[c] Beijing National Laboratory for Condensed Matter Physics, Institute of Physics, Chinese Academy of Sciences, Beijing 100190, China
[d] Shenzhen Institute for Quantum Science and Engineering, Southern University of Science and Technology, Shenzhen 518055, China
[e] International Centre for Quantum Materials, Collaborative Innovation Centre of Quantum Matter, Peking University, Beijing 100871, China
[f] State Key Laboratory for Advanced Metals and Materials, University of Science and Technology Beijing, Beijing 100083, China

ARTICLE INFO

Article history:
Received 26 April 2023
Revised 17 June 2023
Accepted 2 July 2023
Available online 7 September 2023

Keywords:
Electrolytic copper foil
Single-crystallization
Facet copy
Grain growth
Mechanical property

ABSTRACT

Depending on the production process, copper (Cu) foils can be classified into two types, i.e., rolled copper (r-Cu) foils and electrolytic copper (e-Cu) foils. Owing to their high electrical conductivity and ductility at low cost, e-Cu foils are employed extensively in modern industries and account for more than 98% of the Cu foil market share. However, industrial e-Cu foils have never been single-crystallized due to their high density of grain boundaries, various grain orientations and vast impurities originating from the electrochemical deposition process. Here, we report a methodology of transforming industrial e-Cu foils into single crystals by facet copy from a single-crystal template. Different facets of both low and high indices are successfully produced, and the thickness of the single crystal can reach 500 μm. Crystallographic characterizations directly recognized the single-crystal copy process, confirming the complete assimilation impact from the template. The obtained single-crystal e-Cu foils exhibit remarkably improved ductility (elongation-to-fracture of 105% vs. 25%), fatigue performance (the average numbers of cycles to failure of 1600 vs. 200) and electrical property (electrical conductivity of 102.6% of the international annealed copper standard (IACS) vs. 98.5%) than original ones. This work opens up a new avenue for the preparation of single-crystal e-Cu foils and may expand their applications in high-speed, flexible, and wearable devices.

1. Introduction

Owing to the absence of grain boundaries, single-crystal metals demonstrate superior electrical and mechanical properties than polycrystalline ones [1–3], and thus are highly desirable in scientific research and engineering applications. Based on the basic grain growth principle, numerous efforts have been devoted to realizing the single-crystallization of metals [4–7]. Take Cu as an example, to date, large-area single-crystal Cu foils have been synthesized by temperature-gradient-driven [8], contact-free abnormal grain growth [3,9] or seeded growth [10] methods, which greatly promoting their applications in the material synthesis and selective catalysis [8,11–14]. However, the single-crystallization process is found to be highly dependent on the original texture of the Cu foils [3,15,16], and only a few r-Cu foils can be transformed into large single crystals [3]. The universal single-crystallization of Cu foil with any original texture still remains a great challenge and is eagerly waiting to be explored.

In principle, r-Cu foils are produced by repeatedly rolling a thick Cu sheet into a thinner one [17,18], and generally show elongated grains along the rolling direction with a strong texture [3,15,19]. During the recrystallization process, the rotation of the dominant texture component could possibly lead to the formation of single-crystal grains [3,15,19]. It is important to note that not all the r-Cu foils can be transformed into large single crystals, and even a minor deviation in the initial texture may result in the failure of single-crystallization [3]. What's worse, the majority of commercially available Cu foils lack strong textures, which makes them more difficult to be single-crystallized. For example, the most widely used Cu foils, i.e., e-Cu foils, are prepared by electrodeposition of Cu onto a titanium cathode roller [17,18], and the grains in e-Cu foils orient in various directions with a

* Corresponding authors.
E-mail addresses: fuying@sslab.org.cn (Y. Fu), khliu@pku.edu.cn (K. Liu), zhibinzhang@pku.edu.cn (Z. Zhang).

https://doi.org/10.1016/j.jmst.2023.07.039
1005-0302/

loose microstructure [20], forming equiaxed grains with acicular or pyramidal surface morphology [17,21]. In addition, the impurities in the electroplating solution will also be deposited into the e-Cu foils [22]. Thus, even undergoing the same annealing process as the best r-Cu ones, the recrystallized grains will suffer significant competition with each other, and the migration of grain boundaries will be greatly impeded by impurities [23]. As a result, the e-Cu foils always form a coarse-grained polycrystal with an average grain size of several hundred micrometres after annealing [24–26]. Therefore, there is an urgent need to develop a new strategy to realize the single-crystallization of e-Cu foils.

Here, we report a method of transforming industrial e-Cu foils into single crystals by facet copy from single-crystal templates. The introduction of a single-crystal template assimilated the template's lattice into e-Cu foil, allowing the grain orientation transfer of the template Cu to e-Cu. The transferred grains may grow continuously and coalesce with each other to produce a large single-crystal e-Cu foil during the subsequent high-temperature annealing procedure.

2. Experimental

2.1. Preparation of single-crystal e-Cu foils

Original e-Cu foils (18 μm, Nuode New Materials Co. Ltd; 50 μm and 100 μm, Shandong Huiya Metal Technology Co. Ltd) were pressed against onto the single-crystal Cu template. Then a layer of graphite paper with thickness about 20 μm was used to cover the original e-Cu foil, and then a stainless-steel plate or a Cu plate with thickness about 1 cm was put on the graphite paper to create an intimate contact between the original e-Cu foil and the single-crystal Cu template. Finally, they were loaded into a CVD furnace (Tianjin Kaiheng Electric Heating Technology Co. Ltd), and then the system was heated up to 1050 °C in 80 min and held at 1050 °C for 1–5 h. A flow of 500 standard cubic centimetres per minute (sccm) Ar and 50 sccm H_2 was applied throughout the whole annealing process.

2.2. Tensile test

The tensile test was carried out on an electronic universal testing machine (EM6.104, produced by Shenzhen Tesmart Instrument Equipment Co. Ltd) equipped with an optical non-contact extensometer (Red Box-S, produced by Shenzhen Haytham Technology Co. Ltd) and a force transducer (BSA-XS-25kgP, produced by Transcell Technology Inc). Samples used for tensile test were fabricated into dog-bone-shape by laser with a gauge width of 6 mm and length of 10 mm. Before the test, the sample was held on the upper and lower clamps of the force transducer, ensuring that the clamped sample was straight, slightly taut, and not deformed. During the test, the lower clamps remained stationary, while the upper clamps move upward at a constant displacement rate of 0.02 mm/min in the elastic deformation interval and 2 mm/min after the elastic deformation interval. In this process, the force transducer with a measure range of 0–200 N was used to measure the force corresponding to the gauge deformation and the extensometer was used to measure the displacement caused by the gauge deformation, and the data collection rate of the system was set as 10 Hz/s. Finally, the strain will be calculated by the displacement of the gauge and stress can be calculated by the force value.

2.3. Bending fatigue test

The bending fatigue test was carried out on a MIT folding endurance tester (Tianjin Flora Automatic Technology Co. Ltd). The single-crystal e-Cu and original e-Cu foils were fabricated into long strips with size of 8.5 mm × 125 mm and thickness of 40 μm. Before the test, the sample was held on the tester holder, then an upward pulling force of 4.9 N was applied to the sample to keep it in tension. During the test, the lower end of the sample was bent 135° from side to side under bending radius of 2.5 mm at frequency of 175 cycles per minute until the sample completely fracture.

2.4. Electrical test

The electrical conductivity of the samples was measured using the Van der Pauw method on a manual probe station at room temperature. A Keithley 6221 current source and a Keithley nanovoltmeter 2182A were used to supply current and measure voltage respectively. To eliminate the influence of the single-crystal template, the template Cu under the single-crystal e-Cu was removed by electropolishing before the test. Subsequently, the samples were laser-cut into squares with a side length of 1.5 cm for the electrical testing.

2.5. Characterization

Scanning electron microscope (SEM) images were obtained using the Carl Zeiss GeminiSEM 300. The EBSD characterizations were carried out using an Oxford C-Nano instrument. The X-ray diffraction (XRD) 2θ scan was carried out on a Malvern Panalytical Empyrean Series 3 system equipped with a Cu target and a Bruker D8 Advance system equipped with a silver target. XRD φ scan was performed on a Malvern Panalytical Empyrean Series 3 equipped with a Cu target. Laue diffraction were performed on a Photonic Science PSL-Laue backscattering system. Scanning transmission electron microscopy (STEM) and selected-area electron diffraction (SAED) experiments were conducted in an aberration-corrected FEI Titan Themis G2 300 operating at 300 kV. The cross-sectional Cu samples were fabricated using an argon beam polisher (CP, JEOL IB-19530).

3. Results and discussion

In our experiment, we first prepared a large single-crystal Cu foil as the template using "seeded growth technique" [10]. Then we directly pressed the original industrial e-Cu foils onto the single-crystal template, and a metal plate was applied to achieve an intimate contact (step 1 in Fig. 1(a), foil stacking). After being annealed at 1050 °C under a reducing atmosphere for several hours (see Method for more details), the e-Cu foil will transform into a large single crystal with the same surface index as the template (step 2 in Fig. 1(a), facet copy). Using this single-crystal copy strategy, we successfully produced a 35 × 5 cm^2 single-crystal e-Cu foil with the thickness of 18 μm (Fig. 1(b)), which is the largest single-crystal e-Cu foil reported so far (Table 1).

Here, we also directly annealed an original industrial e-Cu foil without the induction of single-crystal Cu template for comparison. The EBSD inverse pole figure mapping along the Z direction (IPF-Z) revealed a colourful pattern, indicating that the direct annealed foil was a polycrystal with grain size of hundreds of microns (Fig. 1(c)). The corresponding XRD 2θ scan displayed multiple peaks (Fig. 1(d)), and the azimuthal off-axis φ scan exhibited numerous rambling peaks (inset in Fig. 1(d)), further confirming the prominent polycrystalline nature of the directly annealed e-Cu foil. In contrast, when utilizing the single-crystal Cu(111) template, the e-Cu foil could be successful transformed into a single crystal. The uniform colour in the EBSD IPF-Z mapping (Fig. 1(e)) and the corresponding XRD 2θ scan data (Fig. 1(f)) confirmed that the facet copy e-Cu was indeed a (111) single crystal. Additionally, the azimuthal off-axis φ scan showed three 120°-equally-separated peaks (inset in Fig. 1(f)), implying that the (111) single crystal does

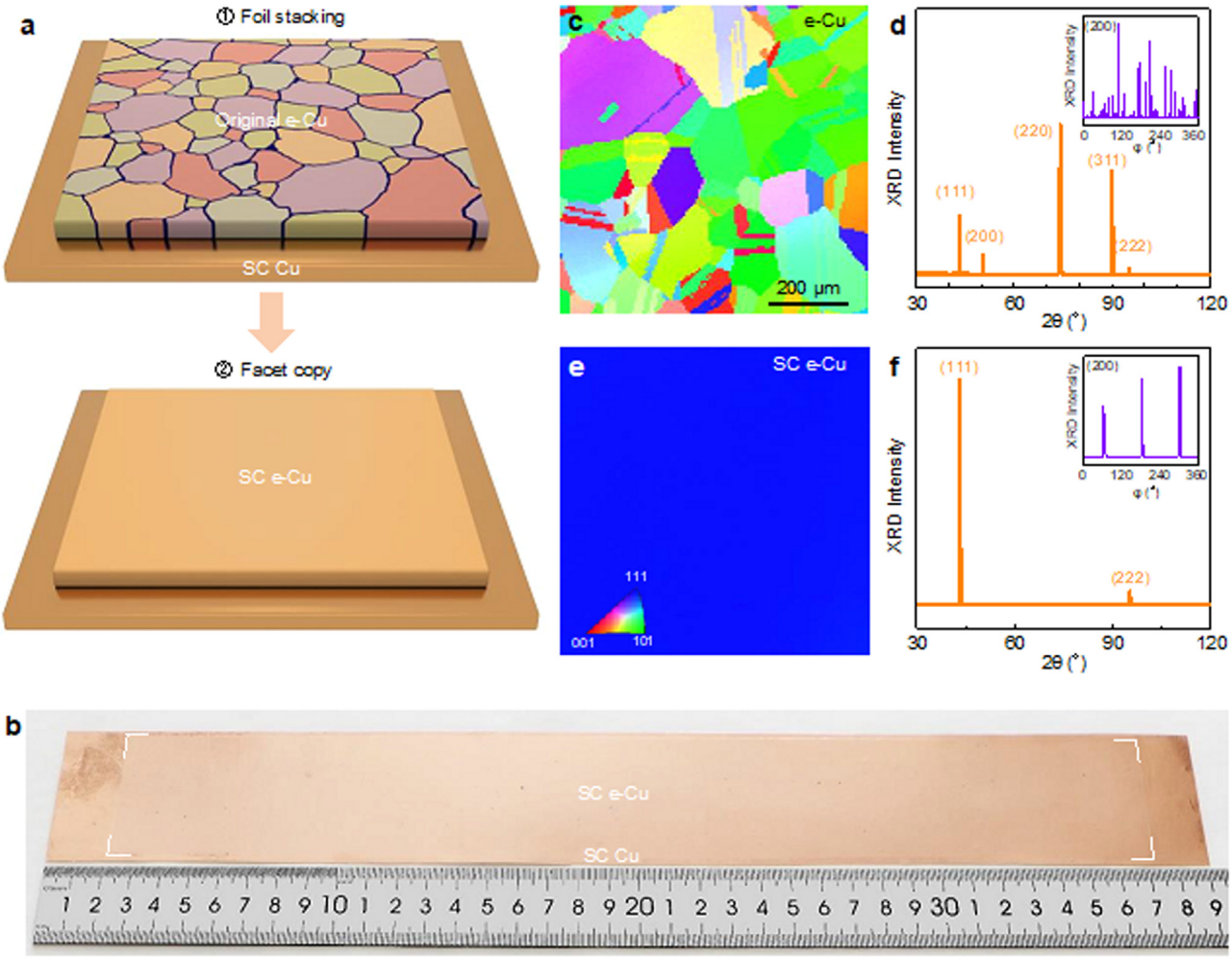

Fig. 1. The facet copy of e-Cu foils. (a) Schematic diagrams of the two steps involved in transforming original e-Cu foil into single crystal. Step 1: stacking original e-Cu foil onto a single-crystal Cu (SC Cu) template. Step 2: facet copy of original e-Cu foil into a single-crystal one after annealing. (b) Optical image of a 35 × 5 cm^2 single-crystal e-Cu copied from a single-crystal Cu template. (c, d) EBSD IPF-Z mapping and XRD 2θ scan spectra (with Cu target) of original e-Cu annealed without single-crystal template. (e, f) EBSD IPF-Z mapping and XRD 2θ scan spectra (with Cu target) of single-crystal e-Cu(111). Inset in (d) and (f), corresponding azimuthal off-axis φ scan spectra.

Table 1
Comparison of the annealed e-Cu foils.

Work	Annealing procedure	Cu thickness	Crystal facet	Typical grain size
Seah et al., J. Vac. Sci. Technol., A 1999, 17, 1963	700 °C, 1 h	38–48 μm	Polycrystal	1 μm
Merchant et al., Mater. Charact. 2004, 53, 335	900 °C, 0.5 h	12–35 μm	Polycrystal	10 μm
Urade et al., Surf. Coat. Technol. 2022, 443, 128606	1050 °C, 6 h	40–60 μm	Polycrystal	50 μm
Jin et al., Science 2018, 362, 1021	1050 °C, 12 h	~23 μm	Polycrystal	500 μm
Our work	1050 °C, 1–5 h	18–500 μm	Single crystal (111), (112), (122), (133), (335), (355)	5–30 cm

not have any in-plane rotation. Further Laue diffraction (Fig. S1), SAED (Fig. S2(a)) and atomically resolved STEM (Fig. S2(b)) results also confirmed the single-crystallinity of the e-Cu(111).

With the facile facet copy design, one can principally obtain single-crystal e-Cu foils with any thickness by repeating the facet copy process. In our experiment, we successfully realized the single-crystallization of e-Cu foils with thickness of 18 μm, 50 μm, 100 μm and up to 500 μm by using a single-crystal Cu(111) template with the thickness of only 25 μm (Fig. S3). The corresponding XRD characterization confirm that the crystal orientation of e-Cu foils is exactly the same as the template (Fig. S4). To better examine the crystal assimilation along the thickness direction, we fabricated the cross-sectional samples using an argon beam polisher. No visible boundary or interface could be observed between e-Cu and the template (Fig. 2(a)). Further EBSD characterizations confirmed that the single-crystal e-Cu foil exhibited the same surface orientations as the template (Fig. 2(b)), demonstrating the successful facet copy of the sample.

What's more, based on the "single-crystal Cu library" we established [10], we can also produce large single-crystal e-Cu foils with

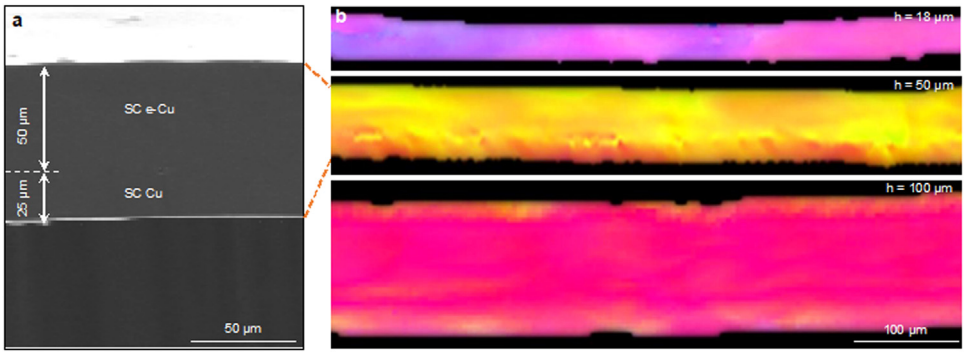

Fig. 2. Single-crystal copy of e-Cu foils with different thickness. (a) The cross-sectional SEM image of a 50-μm-thick single-crystal e-Cu foil templated by a 25-μm-thick single-crystal Cu. (b) Cross-sectional EBSD IPF maps of single-crystal e-Cu foils with thickness *h* of 18 μm, 50 μm and 100 μm templated by a 25-μm-thick single-crystal Cu.

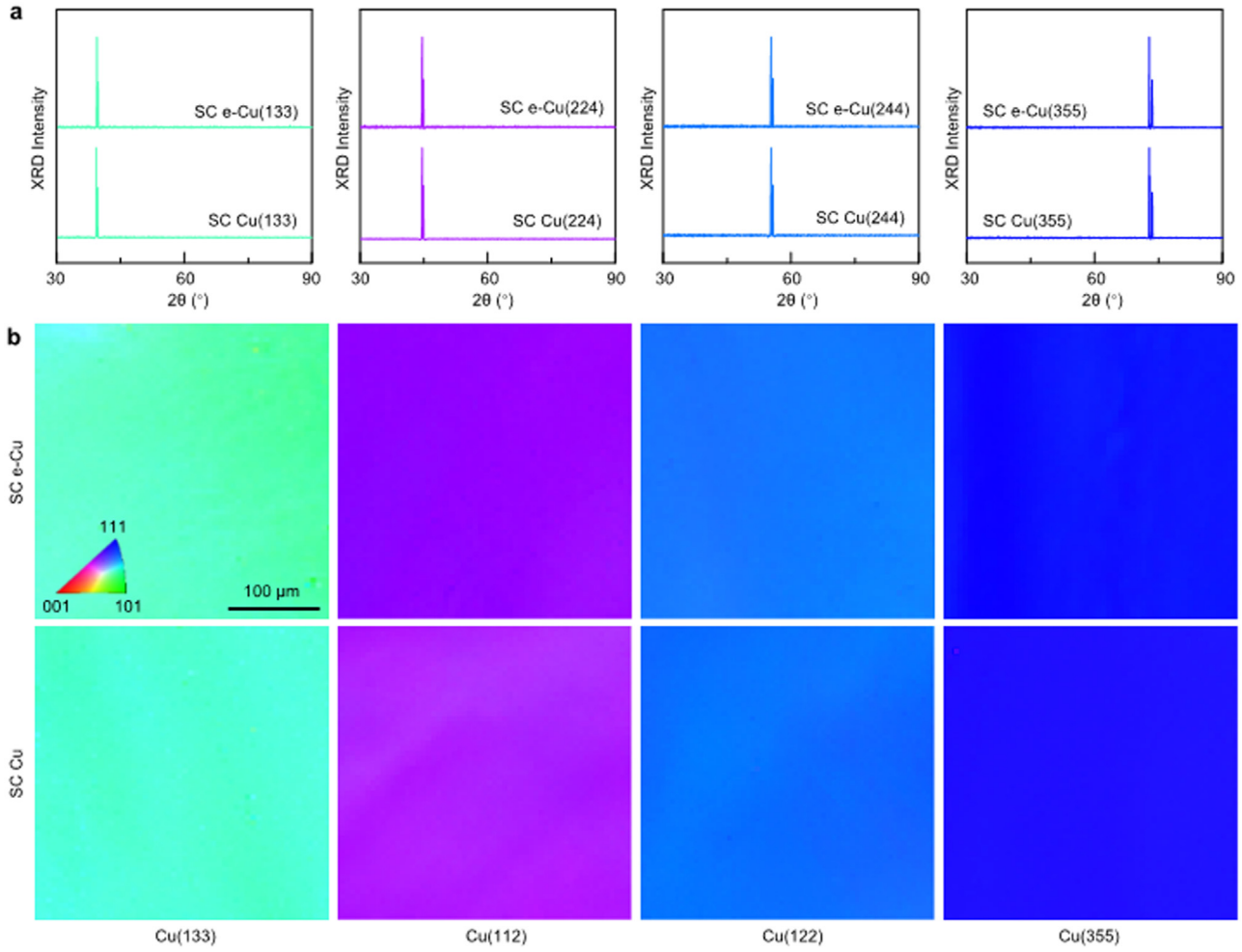

Fig. 3. Single-crystal copy of e-Cu foils with different facet indices. (a, b) XRD 2θ scan spectra (a, with silver target) and corresponding EBSD IPF-Z maps (b) of four kinds of high-index single-crystal e-Cu foils and their corresponding templates.

various surface indices. Besides the Cu(111) single crystals, other four kinds of high-index Cu templates were used to induce the single-crystallization of the e-Cu foils. To identify these high-index facets, an Ag-target XRD with a smaller wavelength was utilized. The XRD results demonstrated that the e-Cu foils exhibited the same peak position with the single-crystal Cu template (Fig. 3(a)). The EBSD IPF-Z mappings revealed that the single-crystal e-Cu foil exhibited the same uniform colour with that of the single-crystal template at a large scale, demonstrating the single-crystallinity of the obtained samples (Fig. 3(b)).

To understand the dynamics of the single-crystal copy strategy, we performed a temperature evolution investigation of the e-Cu grains. As is shown in Fig. S5(a), the surface of original e-Cu foil was very rough, and the grains were oriented at various directions with an average size of several microns. The XRD result (Fig. S5(b)) showed that the original e-Cu was polycrystalline with a weak (220) texture, which is consistent with the EBSD characterization (Fig. S5(c, d)). As the annealing temperature increased, the e-Cu grains gradually grew and fused together, leading to a reduction in surface roughness (Fig. 4(a_1–a_5)). When the annealing time

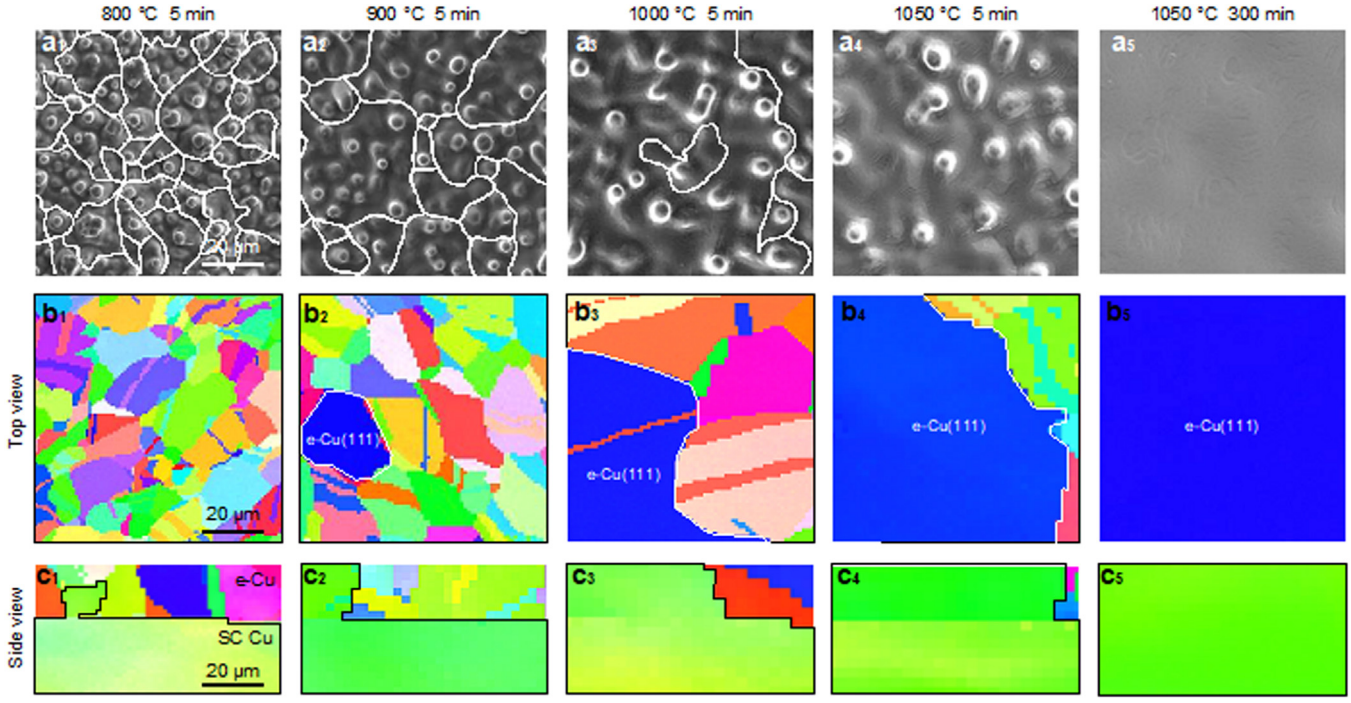

Fig. 4. Grain evolution in the single-crystal copy process. (a) SEM images of the e-Cu foil with the single-crystal Cu(111) template after annealing at 800 °C for 5 min (a_1), 900 °C for 5 min (a_2), 1000 °C for 5 min (a_3), 1050 °C for 5 min (a_4) and 1050 °C for 300 min (a_5). The grain boundaries are indicated by white lines. (b) EBSD maps of the samples obtained from the top view, showing a Cu(111) grain that initially appears and gradually expands to cover the entire area. (c) EBSD maps of the samples obtained from the side view, showing a Cu(111) grain copied from the t-Cu(111) first grew vertically and then spread out. All images in (a) and maps in (b) and (c) have the same scale.

reached 300 min, the surface humps originating from the electrodeposition process were completely eliminated, and the surface appeared uniformly flat, indicating the absence of grain boundaries.

To better probe the facet copy process, we further carried out EBSD characterizations both from the top and the side view direction. After being annealed at 800 °C for 5 min, the grains of e-Cu foil grew larger compared to that of the original e-Cu foil (Fig. 4(b_1)), and a small Cu(111) seed appeared under the induction of the Cu(111) template (Fig. 4(c_1)). With the annealing temperature increases to 900 °C, the Cu(111) grain continued to grow vertically and penetrated the e-Cu foil (Fig. 4(b_2), (c_2)). Further increasing in temperature leads to the grain growth of the (111) seed (Fig. 4(b_3, b_4), (c_3, c_4)), and numerous (111) seeds that appeared separately coalesced with each other (Fig. S6), Finally, a 100% area facet copy of Cu(111) single crystal was achieved through extending the annealing time to 300 min at 1050 °C (Fig. 4(b_5, c_5)). Therefore, the growth, coalescence and template-induced re-orientation of grains are the key points for achieving the single crystallization of e-Cu. When applying the e-Cu foil onto a single-crystal template, grains in the e-Cu would be induced by the template. As a result, numerous small Cu grains will re-orientate into the same direction with the template and grow simultaneously. Finally, they will coalesce with each other to form a large single crystal during the annealing process.

Besides, we would like to suggest that the interfacial stress between the e-Cu foil and the single-crystal Cu template is the main driving force for the single-crystal copy process [15,27,28]. The strongly attached template imposes a huge interfacial stress (estimated to be ~5–50 MPa [28,29]) to the e-Cu foil, and the grains in the e-Cu (~1 μm) are greatly affected by the super large grain (~10 cm) in the template. These grains would nucleate into numerous single-crystal seeds that are same as the template to release the interfacial stress energy [15,30,31]. Therefore, not only Cu(111), which has the lowest surface energy, can copy the surface orientation of the template, but high-index facet e-Cu foils with higher surface energy can also do so.

To evaluate the mechanical performance of single-crystal e-Cu foil, we carried out a series of tensile and bending fatigue experiments. Firstly, the tensile test was conducted using a standard electronic universal testing machine (see Methods section for more details). In order to ensure that the fracture occurred exactly in the middle of the gauge, the samples were fabricated into a dog-bone-shape (Fig. 5(a)). The elongation-to-fracture of single-crystal e-Cu foils (>105%) was about 4 times better than that of the original e-Cu foils (~24%), indicating that the e-Cu foils possess excellent ductility after the single-crystallization (Fig. 5(b)). This substantial improvement in ductility can be attributed to the perfect lattice alignment in the single-crystal structure. For original e-Cu foils, the grains are oriented in virous directions with numerous grain boundaries, hindering the synchronized activation of dislocation slip between grains under uniaxial forces [32]. As a result, the deformation between grains becomes unsynchronized, and stress accumulates at the grain boundaries [33]. When the deformation of individual grains reaches its limit, cracks tend to initiate at the grain boundaries, resulting in inferior elongation-to-fracture of original e-Cu compared to the single-crystal one [28,33].

Furthermore, the bending fatigue test was carried out on a standard folding endurance tester (see Methods section for more details). After repeatedly bending the samples, the single-crystal e-Cu showed superior bending resistance with fracture of more than 1600 cycles, which is 8 times better than that of original e-Cu foil (Fig. 5(c)). It is widely recognized that the bending fatigue test is a low-cycle fatigue test [34] and the plastic performance of Cu foil determines its fatigue life [34,35]. Multiple tests confirmed the effective improvement in the bending fatigue test of the single-crystal e-Cu (Fig. 5(d)), indicating the optimized plastic performance of the single-crystal e-Cu foil. Such superior fatigue per-

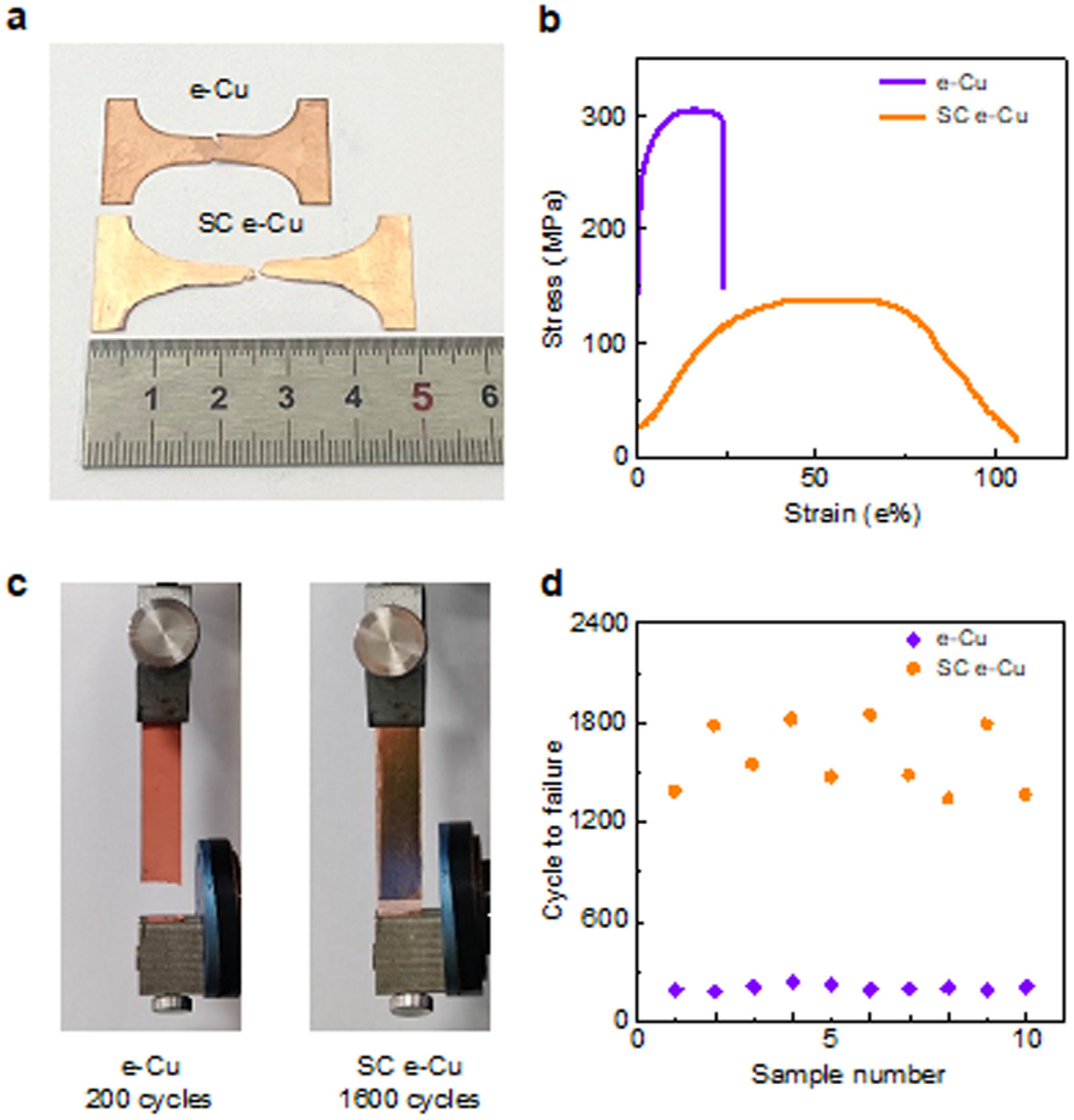

Fig. 5. Mechanical properties of original and single-crystal e-Cu foils. (a) Photograph of the dog-bone-shaped original and single-crystal e-Cu foils after the tensile test. (b) Typical strain-stress curves of original and single-crystal e-Cu foils. (c) Photographs of original and single-crystal e-Cu foils after the fatigue test. (d) Fatigue performance of original and single-crystal e-Cu foils.

formance provides a possibility for its application in advanced flexible and wearable devices [36]. What's more, the electrical property of e-Cu foils was also measured (see Methods section for more details). The result (Fig. S7) showed that the single-crystal e-Cu exhibited an excellent electrical conductivity up to 102.6% IACS, which is much better than that of the original e-Cu (98.5% IACS). This improvement in electrical conductivity further confirms the beneficial impact of single crystallization on the electrical properties of e-Cu foils.

4. Conclusions

In summary, we have developed a strategy that utilizes single-crystal Cu foils as templates to transform e-Cu foils into single-crystal ones. Using this method, we have successfully prepared large-scale single-crystal e-Cu foils with various thickness and surface indices. The produced single-crystal e-Cu foils demonstrate excellent ductility, fatigue performance and electrical property, making them promising in applications of flexible circuits, high frequency circuits, and wearable devices. The main conclusions can be summarized as follows:

(1) Single-crystal e-Cu foils were first realized through a facet copy process, with single-crystal size up to 35 × 5 cm^2, thickness up to 500 μm, and facet type of both low and high indices.
(2) The evolution process of e-Cu foil was directly monitored by crystallographic characterizations, confirming the complete assimilation effect from the template.
(3) The single-crystal e-Cu foils exhibit remarkably improved properties than original ones (elongation-to-fracture: 105% vs. 24%, average numbers of cycles to failure: 1600 vs. 200, electrical conductivity: 102.6% vs. 98.5%).

Declaration of Competing Interest

The authors declare that they have no known competing financial interests or personal relationships that could have appeared to influence the work reported in this paper.

Acknowledgements

This work was financially supported by Guangdong Major Project of Basic and Applied Basic Research (No. 2021B0301030002), the National Natural Science Foundation of China (No. 52025023) and the Key R&D Program of Guangdong Province (No. 2020B010189001).

Supplementary materials

Supplementary material associated with this article can be found, in the online version, at doi:10.1016/j.jmst.2023.07.039.

References

[1] H.C.H. Carpenter, Nature 118 (1926) 266–269.
[2] F.L. Versnyder, M.E. Shank, Mater. Sci. Eng. 6 (1970) 213–247.
[3] S. Jin, M. Huang, Y. Kwon, L.N. Zhang, B.W. Li, S. Oh, J.C. Dong, D. Luo, M. Biswal, B.V. Cunning, P.V. Bakharev, I. Moon, W.J. Yoo, D.C. Camacho-Mojica, Y.J. Kim, S.H. Lee, B. Wang, W.K. Seong, M. Saxena, F. Ding, H.J. Shin, R.S. Ruoff, Science 362 (2018) 1021–1025.
[4] J. Czochralski, Z. Phys. Ohem. 92 (1918) 219–221.
[5] P.W. Bridgman, Proc. Amer. Acad. Arts. Sci. 60 (1925) 305.
[6] R.W.K. Honeycombe, Metall. Rev. 4 (1959) 1–48.
[7] N.K. Mahenderkar, Q.Z. Chen, Y.C. Liu, A.R. Duchild, S. Hofheins, E. Chason, J.A. Switzer, Science 355 (2017) 1203–1206.
[8] X.Z. Xu, Z.H. Zhang, J.C. Dong, D. Yi, J.J. Niu, M.H. Wu, L. Lin, R.K. Yin, M.Q. Li, J.Y. Zhou, S.X. Wang, J.L. Sun, X.J. Duan, P. Gao, Y. Jiang, X.S. Wu, H.L. Peng, R.S. Ruoff, Z.F. Liu, D.P. Yu, E.G. Wang, F. Ding, K.H. Liu, Sci. Bull. 62 (2017) 1074–1080.
[9] Z.C. Li, Y.N. Zhang, Y.W. Duan, D.P. Huang, H.F. Shi, Nanomaterials 11 (2021) 3069.
[10] M.H. Wu, Z.B. Zhang, X.Z. Xu, Z.H. Zhang, Y.R. Duan, J.C. Dong, R.X. Qiao, S.F. You, L. Wang, J.J. Qi, D.X. Zou, N.Z. Shang, Y.B. Yang, H. Li, L. Zhu, J.L. Sun, H.J. Yu, P. Gao, X.D. Bai, Y. Jiang, Z.J. Wang, F. Ding, D.P. Yu, E.G. Wang, K.H. Liu, Nature 581 (2020) 406–410.
[11] M. Cao, D.B. Xiong, L. Yang, S.S. Li, Y.Q. Xie, Q. Guo, Z.Q. Li, H. Adams, J.J. Gu, T.X. Fan, X.H. Zhang, D. Zhang, Adv. Funct. Mater. 29 (2019) 1806792.
[12] L. Wang, X.Z. Xu, L.N. Zhang, R.X. Qiao, M.H. Wu, Z.C. Wang, S. Zhang, J. Liang, Z.H. Zhang, Z.B. Zhang, W. Chen, X.D. Xie, J.Y. Zong, Y.W. Shan, Y. Guo, M. Willinger, H. Wu, Q.Y. Li, W.L. Wang, P. Gao, S.W. Wu, Y. Zhang, Y. Jiang, D.P. Yu, E.G. Wang, X.D. Bai, Z.J. Wang, F. Ding, K.H. Liu, Nature 570 (2019) 91–95.
[13] C.Y. Zhu, Z.B. Zhang, L.X. Zhong, C.S. Hsu, X.Z. Xu, Y.Z. Li, S.W. Zhao, S.H. Chen, J.Y. Yu, S.L. Chen, M. Wu, P. Gao, S.Z. Li, H.M. Chen, K.H. Liu, L.M. Zhang, Chem-Us 7 (2021) 406–420.
[14] C. Liu, Z.H. Li, R.X. Qiao, Q.H. Wang, Z.B. Zhang, F. Liu, Z.Q. Zhou, N.Z. Shang, H.W. Fang, M.X. Wang, Z.K. Liu, Z. Feng, Y. Cheng, H. Wu, D.W. Gong, S. Liu, Z.S. Zhang, D.X. Zou, Y. Fu, J. He, H. Hong, M.H. Wu, P. Gao, P.H. Tan, X.Q. Wang, D.P. Yu, E.G. Wang, Z.J. Wang, K.H. Liu, Nat. Mater. 21 (2022) 1263–1268.
[15] S. Jin, R.S. Ruoff, APL Mater. 7 (2019) 100905.
[16] A.D. Rollett, W.W. Mullins, Scr. Mater. 36 (1997) 975–980.
[17] H.D. Merchant, W. Liu, L.A. Giannuzzi, J.G. Morris, Mater. Charact. 53 (2004) 335–360.
[18] J.L. Zhang, H.B. Chen, B.F. Fan, H.P. Shan, Q. Chen, C.H. Jiang, G.Y. Hou, Y.P. Tang, J. Alloys Compd. 884 (2021) 161044.
[19] M. Judelewicz, H.U. Kunzi, N. Merk, B. Ilschner, Mater. Sci. Eng. A 186 (1994) 135–142.
[20] L. Lu, X. Chen, X. Huang, K. Lu, Science 323 (2009) 607–610.
[21] X.Q. Yin, L.J. Peng, S. Kayani, L. Cheng, J.W. Wang, W. Xiao, L.G. Wang, G.J. Huang, Rare Met. 35 (2016) 909–914.
[22] M. Stangl, J. Acker, S. Oswald, M. Uhlemann, T. Gemming, S. Baunack, K. Wetzig, Microelectron. Eng. 84 (2007) 54–59.
[23] S.H. Brongersma, E. Kerr, I. Vervoort, A. Saerens, K. Maex, J. Mater. Res. 17 (2002) 582–589.
[24] S. Nakahara, C.Y. Mak, Y. Okinaka, J. Electrochem. Soc. 138 (1991) 1421–1424.
[25] Z.Y. Zhang, Y.W. Wu, Y.M. Zhang, T. Hang, A.M. Hu, H.Q. Ling, M. Li, J. Electrochem. Soc. 166 (2019) D577–D582.
[26] A.R. Urade, K.N.C. Kumar, N.V. Pulagara, I. Lahiri, K.S. Suresh, Surf. Coat. Technol. 443 (2022) 128606.
[27] J. Greiser, D. Muller, P. Mullner, C.V. Thompson, E. Arzt, Scr. Mater. 41 (1999) 709–714.
[28] C.V. Thompson, R. Carel, J. Mech. Phys. Solids 44 (1996) 657–673.
[29] R. Abermann, R. Koch, Thin Solid Films 129 (1985) 71–78.
[30] M. Murakami, M. Moriyama, S. Tsukimoto, K. Ito, Mater. Trans. 46 (2005) 1737–1740.
[31] R.D. Doherty, D.A. Hughes, F.J. Humphreys, J.J. Jonas, D.J. Jensen, M.E. Kassner, W.E. King, T.R. McNelley, H.J. McQueen, A.D. Rollett, Mater. Sci. Eng. A 238 (1997) 219–274.
[32] A. Tatschl, O. Kolednik, Mater. Sci. Eng. A 342 (2003) 152–168.
[33] Z.Q. Cui, B.X. Liu, in: Metallurgy and Heat Treatment Theory, 3rd ed., Harbin Institute of Technology Press, Haerbin, 2007, pp. 158–164. (in Chinese).
[34] , in: X.H. Yang, C.Y. Chen (Eds.), Fracture and Fatigue, 2nd ed., Huazhong University of Science and Technology Press, Wuhan, 2018, pp. 75–81. (in Chinese).
[35] T. Hatano, Y. Kurosawa, J. Miyake, J. Electron. Mater. 29 (2000) 611–616.
[36] A. Nozariasbmarz, H. Collins, K. Dsouza, M.H. Polash, M. Hosseini, M. Hyland, J. Liu, A. Malhotra, F.M. Ortiz, F. Mohaddes, V.P. Ramesh, Y. Sargolzaeiaval, N. Snouwaert, M.C. Ozturk, D. Vashaee, Appl. Energy 258 (2020) 114069.